

Dynamic observation of circRNA and mRNA profiles in a rat model of deep vein thrombosis

BAOLAN SUN^{1*}, XI CHENG^{2*}, MU ZHANG³, QIN SHI²,
XINXIN ZHAO², XUDONG WANG¹ and YUQUAN ZHANG²

Departments of ¹Laboratory, ²Gynecology and Obstetrics, and ³Ophthalmology,
Affiliated Hospital of Nantong University, Nantong, Jiangsu 226001, P.R. China

Received January 31, 2023; Accepted July 20, 2023

DOI: 10.3892/etm.2023.12166

Abstract. The goal of the present study was to identify different transcriptome expression profiles involved in the pathogenesis of deep vein thrombosis (DVT), and to illustrate the diagnostic and therapeutic potential of circular RNAs (circRNAs) and mRNAs in DVT progression. A Sprague-Dawley rat model of DVT was successfully established through the stenosis method and samples were sequenced at four time points (1, 6 and 12 h, and 3 days after ligation) to observe the dynamic changes in circRNAs and mRNAs during DVT progression. RNA sequencing was used to analyze the circRNA and mRNA expression profiles, and associated functions and pathways, in the blood of DVT rats at the four time points. In addition, Short Time Series Expression Miner (STEM) analysis was performed to explore temporal gene expression. Differential expression of 1,680, 4,018, 3,724, and 3,036 circRNAs, and 400, 1,176, 373, and 573 mRNAs was observed in the 1, 6 and 12 h, and 3-day groups, respectively, compared with the sham group (fold change >2.0 or <-2.0, P<0.05). Functional enrichment analysis indicated that differentially expressed mRNAs were associated with the following terms: Immune response, cell activation, blood stasis facilitated organelle, extracellular membrane-bounded organelle, and blood microparticle, oxygen transporter activity. STEM analysis indicated that the expression of 366 circRNAs in circRNA profile 45 and 270 mRNAs in mRNA profile 45 was consistent with thrombus progression.

Enrichment analysis was performed on mRNA profile 45. The main Gene Ontology annotations were chromosome segregation, mitotic sister chromatid segregation, cell cycle process, and ligand-dependent nuclear receptor transcription coactivator activity. Pathway enrichment analysis identified the platelet-associated pathway, immune-associated pathway, and inflammation-relation pathway. According to the enriched platelet-associated pathways, four mRNAs and ten candidate circRNAs were selected for reverse transcription-quantitative PCR verification. The expression of nine of the ten circRNAs and all four mRNAs was consistent with the sequencing results. In summary, differentially expressed circRNAs and mRNAs are dynamically involved in DVT development. Dysregulated transcriptome profiles and the corresponding functions and pathways may provide mechanistic insights into DVT diagnosis and treatment.

Introduction

Deep vein thrombosis (DVT) is caused by the abnormal coagulation of blood in the deep veins, thus leading to lumen stenosis and obstruction of the venous return. DVT is the third major cardiovascular cause of death and/or disability after ischemic cardiomyopathy and stroke, and its incidence is increasing each year. Clinically, 90% of cases of venous thromboembolism (VTE) are due to DVT (1,2). The onset of DVT is insidious, sudden and is mostly asymptomatic. However, delayed diagnosis and treatment may lead to pulmonary embolism and post-thrombotic syndrome, or even death (3). A recent study has suggested that conventional pharmacologic prophylaxis may not be sufficient to prevent the development of VTE in patients with severe coronavirus infection (4). D-dimer is the clinical biomarker most commonly used to exclude a diagnosis of DVT, with high sensitivity but low specificity (5). Therefore, further studies are needed to explore the mechanisms of DVT initiation and progression, to provide patients with improved diagnosis and treatment strategies.

Circular RNAs (circRNAs) belong to a novel class of regulatory non-coding RNAs. In contrast to linear RNAs, with 5' terminal caps and 3' tails, the ends of circRNAs are covalently linked, thus forming a closed circular structure that renders them more stable than their linear counterparts (6,7). This molecular structure allows circRNAs to act as microRNA

Correspondence to: Professor Xudong Wang, Department of Laboratory, Affiliated Hospital of Nantong University, 20 Xisi Road, Nantong, Jiangsu 226001, P.R. China
E-mail: wangxudong88@Hotmail.com

Professor Yuquan Zhang, Department of Gynecology and Obstetrics, Affiliated Hospital of Nantong University, 20 Xisi Road, Nantong, Jiangsu 226001, P.R. China
E-mail: jsnt_zhangyuquan@163.com

*Contributed equally

Key words: circular RNA, deep vein thrombosis, mRNA, RNA sequencing, short time series expression miner

(miRNA) sponges, by regulating transcription or splicing, interacting with RNA-binding proteins, and participating in gene expression regulation. Therefore, circRNAs may potentially have broad applications in clinical diagnosis and treatment (8-10).

To date, numerous studies have shown that circRNAs are closely associated with the diagnosis and treatment of cardiovascular diseases, and certain circRNAs have been identified as cardiovascular disease biomarkers (11-15). Recently, circRNAs have been reported to accelerate lower extremity DVT via sponging miRNA, thus regulating mRNA expression (16,17). Although circRNAs have been suggested to be involved in the pathogenesis and regulatory mechanism of DVT, few studies have examined the global dynamic changes in circRNAs and mRNAs during DVT progression.

To address this issue, the dynamic changes in circRNAs and mRNAs during the development of DVT were investigated, in a rat model by performing RNA sequencing. Differentially expressed genes encoding circRNAs and mRNAs were detected and it was predicted how these RNAs may function through bioinformatics analysis. Short Time Series Expression Miner (STEM) and circRNA-mRNA regulatory network analyses were also conducted. Furthermore, the expression of key circRNAs was verified by reverse transcription-quantitative PCR (RT-qPCR). The identification of DVT-associated key circRNAs may contribute to DVT diagnosis and treatment.

Materials and methods

Construction of the DVT rat model. A total of 90 male Sprague-Dawley rats (weight, 250-300 g; age, 10-12 weeks) were obtained from the Experimental Animal Center of the Medical College of Nantong University (Nantong, China) [SCXK (Su) 2014-0001]. The rats were kept under a 12-h light/dark cycle, a temperature of $23\pm3^{\circ}\text{C}$, and a humidity of 55-60%, and were given free access to food and water. The present experiment was approved (approval no. 20170930-001) by the experimental animal ethics committee of Nantong University (Nantong, China). A stasis-induced venous thrombosis model was implemented as previously described (18,19). Briefly, the rats were anesthetized by intraperitoneal injection of 0.3% pentobarbital sodium (30 mg/kg) and placed in supine position. After a midline laparotomy, the intestines were exteriorized and placed to the left of the animal. The inferior vena cava (IVC) was carefully separated from the surrounding tissues and partially ligated just below the renal veins, along with complete ligation of all visible side branches. The rats were allowed to recover post-surgery and housed under a 12-h light/dark cycle, a temperature of $23\pm3^{\circ}\text{C}$, and a humidity of 55-60%, and were given free access to food and water during recovery. Finally, the rats were sacrificed at 0.5, 1, 2, 4, 6, 8, 12 and 24 h, and 2, 3, 7, 14 or 21 days after the operation. Before sacrifice, a total of 2 ml venous blood was collected from the suprarenal IVC into EDTA-coated capillary tubes for next-generation sequencing after the model rats were anesthetized in an isoflurane chamber (3-4%) and maintained with a face mask using 1-2% isoflurane. All rats were sacrificed by cervical dislocation under deep anesthesia with 2% isoflurane. Subsequently, the thrombosed IVC was carefully dissected, and the thrombus was extracted. The weight (g) and length

(cm) of thrombi harvested from the IVC were measured with an electronic balance (Shanghai Mettler Toledo Co., Ltd.) and Vernier calipers (Deli Co., Ltd.). The IVC plus thrombus was fixed immediately in formalin and stained with hematoxylin and eosin (H&E). A total of six rats were included in each time point and the sham group, in which suture lines were passed, but no blood vessels were ligated. The main IVC and branches from rats in the sham group were separated by laparotomy and treated in the same manner as those from the model rats.

Histological examination. After extraction, the IVCs plus thrombi were collected in 10% buffered formalin, embedded in paraffin, serially cross-sectioned at $5\text{ }\mu\text{m}$, and stained with H&E (20 min in hematoxylin solution and 60 sec in eosin solution at room temperature), according to standard procedures. All histological images were acquired with an inverted microscope (Motic (Xiamen) Electric Group Co., Ltd.) and analyzed in Motic Images 2.0 software.

Total RNA isolation, library construction and sequencing. Total RNA from cells obtained from the IVC was extracted with TRIzol[®] reagent (cat. no. 15596-026; Invitrogen; Thermo Fisher Scientific, Inc.) and analyzed with an Agilent 2100 BioAnalyzer (Agilent Technologies, Inc.) and Qubit fluorometer (Invitrogen; Thermo Fisher Scientific, Inc.). Samples with an RNA integrity number >7.0 and a 28S:18S ratio >1.8 were used in subsequent experiments. Libraries were generated and sequenced by CapitalBio Technology, Inc. A total of $5\text{ }\mu\text{g}$ RNA per sample was used as input material for RNA sample preparation. First, ribosomal RNAs were depleted with an Epicentre Ribo-zero[™] rRNA Removal kit (cat. no. RZH1046; Epicentre; Illumina, Inc.) to obtain rRNA-depleted RNAs, which were further treated with RNase R (cat. no. RNR07250; Epicentre) and subjected to TRIzol extraction. Sequencing libraries were then generated with the rRNA-depleted and RNase R-digested RNAs and a NEBNext[®] Ultra[™] Directional RNA Library Prep kit (cat. no. E7530S; New England Biolabs), according to the manufacturer's recommendations. Briefly, fragmentation was performed with divalent cations under elevated temperature in NEBNext First Strand Synthesis Reaction Buffer. First-strand cDNA was synthesized with random hexameric primers and M-MuLV reverse transcriptase (RNaseH). Second-strand cDNA was subsequently synthesized with DNA polymerase I and RNase H. In the reaction buffer, dNTPs with dTTP were replaced by dUTP. Remaining overhangs were converted into blunt ends via exonuclease/polymerase activity. After adenylation of the 3' ends of the DNA fragments, an NEBNext Adaptor with a hairpin loop structure was ligated for hybridization. To select cDNA fragments 150-200 bp in length, the library fragments were purified with an AMPure XP system (Beckman Coulter, Inc.), then performed treatment with 3 μl USER Enzyme (cat. no. M5505; New England Biolabs) with size-selected, adaptor-ligated cDNA at 37°C for 15 min, then 5 min at 95°C , before PCR. PCR was performed with Phusion High-Fidelity DNA polymerase, Universal PCR primer, and Index (X) Primer. Finally, the library was purified (AMPure XP system), and quality was assessed with an Agilent Bioanalyzer 2100 system. The library preparations were sequenced on the Illumina HiSeq XT platform, and 300-bp paired-end reads were generated.

RNA-sequencing data analysis. Raw reads (in FASTQ format) were processed with FASTQ and fastp. Clean reads were then obtained by removal of adapter-containing, poly-N-containing, and low-quality reads from the raw data. The Q20, Q30 and GC content of the clean data were calculated. All downstream analysis was based on the resulting high-quality clean data. Reference genome and gene annotation data were downloaded from the NCBI genome website (<https://www.ncbi.nlm.nih.gov/pmc/>). An index of the reference genome was built with Bowtie v2.0.6 (20), and paired-end clean reads were aligned to the reference genome with Tophat2. Unmapped reads were retained, and 20-mers from the 5' and 3' ends of these reads were extracted and aligned independently to reference sequences with Tophat2. Anchor sequences were extended with *find circ*, such that the complete read was aligned, and the breakpoints were flanked by GU/AG splice sites. The back-spliced reads with at least two supporting reads were then annotated as circRNAs. Expression levels of circRNAs were normalized by spliced reads per billion mapped reads as follows: Normalized expression=(back-spliced reads) $\times 10^9$ /(total reads). Differential expression between groups was determined with *limma* (21). The default threshold P-value for differential expression was set to 0.05 and \log_2 (fold change)>1.

STEM. STEM defines a set of distinct and representative model temporal expression profiles independently of the data, which correspond to possible profiles of changes in gene expression over time. The number of genes expected to be assigned to a profile is estimated by randomly permuting the original time point values, renormalizing the gene expression values, assigning genes to their most closely matching model profiles, and repeating the process for numerous permutations. Statistically significant model profiles that are similar to one another can be grouped into clusters. A color fill indicates a significant profile, and each color indicates a different cluster. The biological significance of the set of genes assigned to the same profile or the same cluster of profiles can then be assessed with enrichment analysis. For identification of genes temporally coregulated and clustering with the phenotypic parameters, the STEM software tool was used (STEM, version 1.3.10; Jason Ernst; <http://www.cs.cmu.edu/~jernst/stem/>). STEM was run with the 'normalize data' option, with all other settings set to the default.

Gene ontology (GO) annotations and Kyoto Encyclopedia of Genes and Genomes (KEGG) pathway analysis. The differential expression of mRNAs was analyzed to further investigate their biological functions and pathways according to GO functional annotation and KEGG pathway analysis (<https://www.genome.jp/kegg/>) with the cluster Profiler R package 4.0 (22) GO terms and KEGG pathways with corrected $P < 0.05$ were considered significantly enriched.

RT-qPCR. Total RNAs in blood samples were extracted with TRIzol reagent. RNA concentration and purity were measured spectrophotometrically by absorbance measurements at 260 and 280 nm using the NanoDrop ND-1000 (Thermo Fisher Scientific, Inc.). OD260/OD280 ratios between 1.8 and 2.0 were deemed acceptable. RNA was reverse transcribed into cDNA with a High-Capacity cDNA Reverse Transcription kit (cat. no. 4368814; Thermo Fisher Scientific, Inc.) according to the

Table I. Reverse transcription-quantitative PCR primers for candidate mRNAs and circRNAs.

mRNA/ circRNA name	Sequence (5'-3')
Lgals3bp	F: TGGTCTGCTCCAACGATTCC R: GTCCTGCTGGCTGTCAAAGA
Kif18a	F: CAGCCAAGTTGTCGCGGT R: TGTGAGTCTTCCCAGATCCAGT
Kif4a	F: TAAACTCCGAAGGCGCACAT R: GCGTTGTTTTGGCTGGTCTT
Tuba4a	F: AGACGTACATCCCAAACATCATC R: AAGGAGTCATCCCCTCCACC
CBT15_	F: CGGGTCTGGCCATTTTACATC
circR_3235	R: CAGCAACAGCTCTAACATCGT
CBT15_	F: TTGGGGATGTCTGCTTGTGTA
circR_31289	R: GCAGGATGGTGACAGATTGC
CBT15_	F: CCGCCCACCAATCTCCAAAG
circR_4786	R: TGCCAGGTTTCATTTCTGTC
CBT15_	F: GCGACTCTGATGACTCTCTCC
circR_33780	R: CTGCGGCTCATTACAAATCTC
CBT15_	F: ATTGACGTCTAGCATGTTTTCT
circR_14797	R: TCACCACGATGTTGGAGGG
CBT15_	F: AGGAGTTGGAGAAAACCTTGA
circR_2763	R: GACCACATCCGTAAACTGGG
CBT15_	F: TCTTTGCAATATGATTGGACTTGAT
circR_14565	R: AGCAAGTTCTTGGCTGGACT
CBT15_	F: AAGTCTGTGGGCATCGGAGAG
circR_16149	R: CAGTGGAGAGGGAAGTGCCTA
CBT15_	F: ACTATGGCAGCCCACCTAAC
circR_40422	R: GTGATCAGGTGCAAGGTGTCT
CBT15_	F: AAAAGGAAGGAGCTACACCGAG
circR_22738	R: CATCCCACACTGGTGCAAA
GAPDH-Rat	F: AGTGCCAGCCTCGTCTCATA R: AACTTGCCGTGGGTAGAGTC

F, forward; R, reverse; circ-, circular.

manufacturer's protocol. RT-qPCR was performed with TaqMan Multiplex Real-Time Solution (cat. no. 446188;1 Thermo Fisher Scientific, Inc.) according to the manufacturer's protocol, with GAPDH expression serving as an endogenous control. Briefly, the RT-qPCR cycling protocol consisted of enzyme activation at 95°C for 10 min, 40 cycles of denaturation at 95°C for 15 sec, and annealing and extension at 60°C for 1 min, with melting curve analysis (temperature ramp 2%) at 60-95°C. On the basis of the sequences of circRNAs, primers were designed for the candidate circRNAs across a splice site (back-splice), owing to the loop forming characteristic of the circRNAs. Primer 5.0 (www.premierbiosoft.com/primerdesign/index.html) was used to design specific primers for candidate mRNAs and circRNAs (primer sequences are listed in Table I). RT-qPCR was performed with an ABI 7500 Real-Time PCR system (Applied Biosystems; Thermo Fisher Scientific, Inc.). Each relative RNA expression level was calculated from three separate

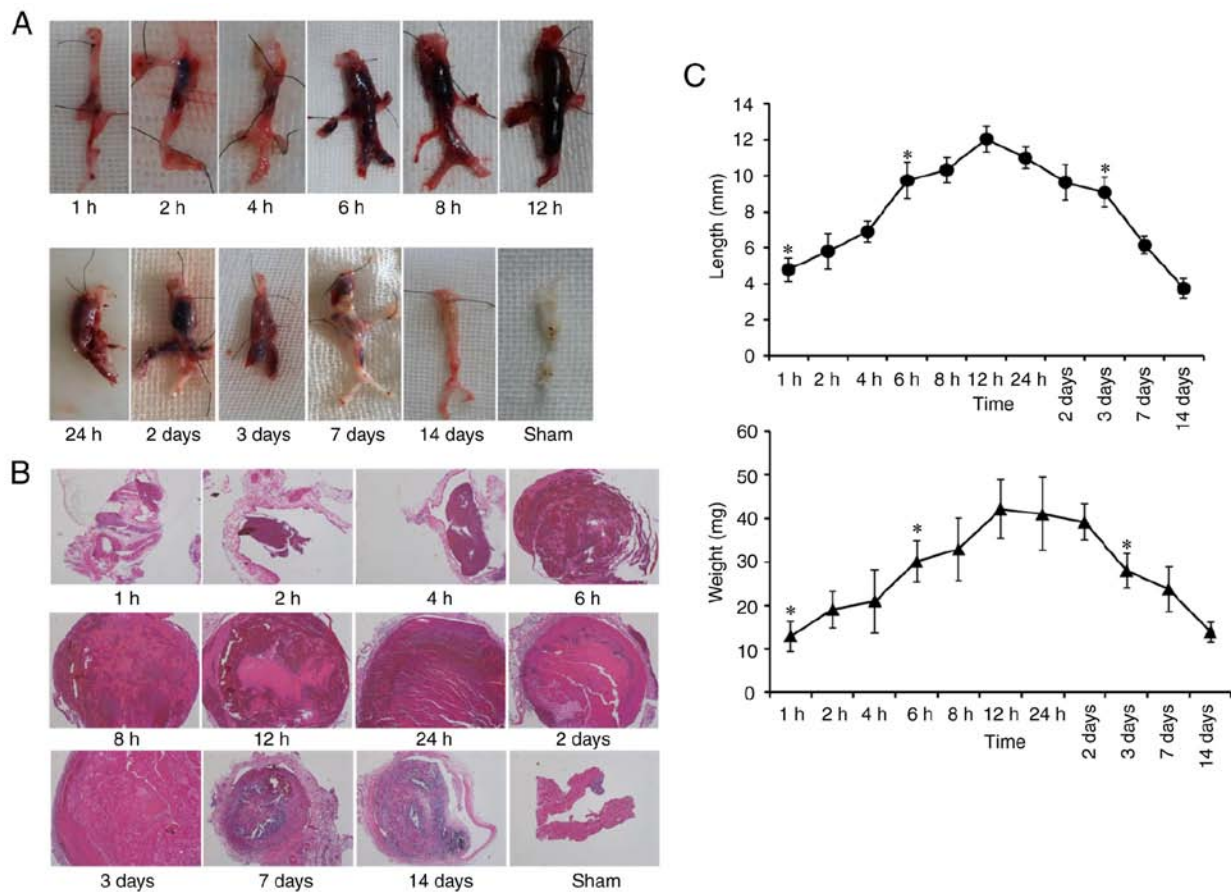


Figure 1. Dynamic observation of DVT progression in rat model. (A) Inferior vena cava thrombus gross map of DVT model group at each time point. (B) Hematoxylin-eosin staining of thrombus at each time point in DVT model group (magnification, x10). (C) The weight or length of the thrombus varies with time. * $P < 0.05$. DVT, deep vein thrombosis.

experiments. The relative expression levels of circRNAs and mRNAs were determined with the $2^{-\Delta\Delta C_q}$ method (23).

Databases. To further confirm the presence of the verified circRNAs, CIRCpedia-V2 (<https://www.biosino.org/circpedia/>), an updated comprehensive database containing circRNA annotations across six different species, was used. To identify human circRNAs that are homologous to the key circRNA, circBase (<http://www.circbase.org>) was used. miRNAs binding both the circRNA and the mRNA were screened with MiRdb (<https://mirdb.org>) and TargetScan (https://www.targetscan.org/vert_80/).

Statistical analysis. The data were processed in SPSS 22.0 statistical software (IBM Corp.). Measured data are expressed as the mean \pm standard deviation. Unpaired data with a normal distribution and homogeneity of variance between two groups were compared with unpaired t-tests, and multiple groups were compared with one-way analysis of variance (ANOVA) followed by Tukey's test. $P < 0.05$ was considered to indicate statistically significant difference.

Results

Dynamic observation of DVT progression in the rat model. A rat model was successfully established of DVT by stenosis.

Rats were divided into 13 DVT groups (0.5, 1, 2, 4, 6, 8, 12 and 24 h; and 2, 3, 7, 14 and 21 days) and a sham group, with six rats per time point, except in the 1 h group, which included eight rats (Table SI). The model was successfully established in 86 rats, and four rats succumbed (one each because of excessive bleeding during operation, anesthetic overdose, sudden death, or intestinal obstruction).

At 2 h post-operation, the vein distal to the partial ligation appeared dark red, and a coagulation-like substance formed in the lumen, which moved when light pressure was applied to the tube wall. At 6 h post-operation, the color of the ligated vein had deepened, the vein wall became tough and less elastic, and the hardness of the clot increased. At 12 h, the partial ligated distal vein was black and red, the internal thrombus was tough, the activity of the model vein decreased, and the mesenteric vein was dilated. After 3 days, careful separation and exposure of the model segment vein revealed that the blood vessel and embolus were dark and stiff, the color of the tube wall was pale, and the clot in the lumen adhered to the tube wall (Fig. 1A). In the sham-operated group, the activities of both hind limbs were normal at all time points, the diameter of the IVC remained unchanged, and the blood was dark red and flowed smoothly. The vascular wall was soft and elastic, the mesenteric veins were uniform in thickness with no abnormal expansion, and no thrombosis was observed.

HE staining indicated that the IVC was not completely thrombosed at 1 h after model establishment. Over time, the blood flow stagnated, and the thrombus grew an embolus that completely blocked the vessel by 6 h, thus indicating wetting, smoothness, softness, and elasticity. With prolongation of the modeling time from 6–48 h, the thrombus dried out, and developed cracks and fibrosis, although it still filled the entire vessel. Thrombus organization was observed on day 3, and HE staining showed clear organization, desiccation, pyknosis, and disintegration of the thrombus on days 7 and 14 (Fig. 1B).

Gross observation and HE staining of the thrombi revealed differences in the percentage thrombus formation at each time point, with 0% (0/6 at 0.5 h; 75% (6/8) at 1 h; 100% (48/48) at 2, 4, 6, 8, 12 and 24 h, and 2 and 3 days; 83.3% (10/12) at 7 and 14 days; and 50.0% (3/6) at 21 days (Table SI).

Thrombus length and weight are important parameters in thrombus research. As shown in Fig. 1C, the initial stage of thrombosis occurred from 1 to 6 h, the stable stage occurred from 6 to 48 h, and the thrombus diminished or became organized after 3 days. Thrombus formation began at 1 h after model establishment, and no significant differences in thrombus length or weight were observed at 2 and 4 h ($P>0.05$). Thrombus length and weight increased significantly at 6 h and were significantly higher at 6–48 h than 2–4 h ($P<0.05$). However, no significant differences were observed among thrombi at 6, 8, 12, 24 and 48 h ($P>0.05$). A total of three days after the operation, the thrombus had clearly diminished, and the length and weight of thrombus had decreased significantly with respect to those at 48 h ($P<0.05$). Thrombus resolution continued, and by day 7, no thrombus was observed in 1 of the 6 DVT rats.

Given that 1, 6 and 12 h, and 3 days appeared to be the key time points of thrombosis progression, blood samples were collected from the model rats at those time points and next-generation sequencing of circRNAs and mRNAs was performed.

Global expression profiles of circRNAs and mRNAs in distinct developmental stages of DVT. CircRNA expression profiles are presented as a volcano plot (Fig. 2A–D). A total of 1,680, 4,018, 3,724 and 3,036 circRNAs were differentially expressed in model rats at 1, 6 and 12 h, and 3 days, respectively, compared with sham group rats (fold change >2.0 or <-2.0 , $P<0.05$), of which 736, 3,691, 3,406 and 2,639 were upregulated, and 944, 327, 318 and 397 were downregulated. The most common type of circRNA was exon type. The numbers of in-gene, intron, and intron and exon type circRNAs were lowest (4, 21 and 5, respectively). Of the upregulated circRNAs, 85 were detected at all time points, according to Venn analysis. Among the downregulated circRNAs, 138 were detected at all time points, according to Venn analysis (Fig. S1A–D).

Expression profiles of mRNA are presented as a scatter-plot (Fig. 3A–D). A total of 400, 1176, 373, and 573 mRNAs were differentially expressed in model rats at 1, 6 and 12 h, and 3 days, respectively, compared with the sham group (fold change >2.0 or <-2.0 , $P<0.05$), of which 169, 885, 298 and 500 were upregulated, and 231, 291, 75 and 73 were downregulated. The top 20 up- and downregulated genes at 1, 6 and 12 h, and 3 days are shown in Table SII. Of the upregulated mRNAs, 69 were expressed at all time points, according to Venn analysis.

None of the downregulated mRNAs were expressed at all time points, according to Venn analysis (Fig. S2A–C).

Enrichment analysis of differentially expressed mRNAs at different stages of DVT. To further investigate the roles of mRNAs in DVT development, functional enrichment analyses of genes was performed, including GO and KEGG analyses. As shown in Fig. 4A–D, GO analysis of differentially expressed mRNAs in the 1 h group compared with the sham group indicated that the top 20 significantly enriched biological processes (BPs), cellular components (CCs), and molecular functions (MFs) included positive regulation of immune system process, immune response, and cell activation. Additionally, these BPs were enriched 6 and 12 h, and 3 days after operation. For annotations of CCs, the terms of organelle, cytoplasm, extracellular membrane-bounded organelle and blood microparticle were enriched. For MF terms, annotations for protein binding, oxygen transporter activity and catalytic activity were highly enriched.

KEGG analysis of differentially expressed mRNAs in the 1, 6, and 12 h, and 3-day groups compared with the sham group indicated that the most enriched pathways were influenza A, metabolic pathways, phagosome and metabolic pathways (Fig. 5A–D).

STEM analysis of differentially expressed circRNAs and mRNAs and STEM-Enrichment analysis. To address the circRNA and mRNA expression patterns at different stages of DVT, STEM analysis was performed. Consequently, 50 profiles of circRNAs and mRNA were identified. Among them, 10 circRNA profiles and 11 mRNA profiles were significantly expressed ($P<0.05$). The black line in each profile represents the expression pattern of the genes at different times (Figs. 6A and 7A). Of note, among all profiles determined, profile 45 involved 366 circRNAs (Fig. 6B), and profile 45 of involved 270 mRNAs (Fig. 7B), in agreement with the observed trend in thrombus weight/length.

To identify the major functions and signaling pathways of profile 45 of mRNA, GO annotation and KEGG pathway analyses were performed. The most significantly enriched BP, CC and MF terms of mRNAs in profile 45 were chromosome segregation, mitotic sister chromatid segregation, cell cycle and ligand-dependent nuclear receptor transcription coactivator activity (Fig. 7C). Pathway analysis of profile 45 indicated enrichment in platelet-associated pathways (factors involved in megakaryocyte development and platelet production, platelet degranulation, response to elevated platelet cytosolic Ca^{2+} , platelet activation, signaling and aggregation, and platelet activation); immune-associated pathways (adaptive immune system, immune system, autoimmune thyroid disease, regulation of innate immune responses to cytosolic DNA, cytokine signaling in immune system and innate immune system); and inflammation-relation pathways (inflammation mediated by chemokine and cytokine signaling pathway, herpes simplex infection, HTLV-I infection and Epstein-Barr viral infection involved in inflammatory pathways; Fig. 7D).

Screening of candidate differential expression circRNAs and mRNAs. Because platelets have been found to be a major factor in the formation of thrombosis (24), platelet-associated

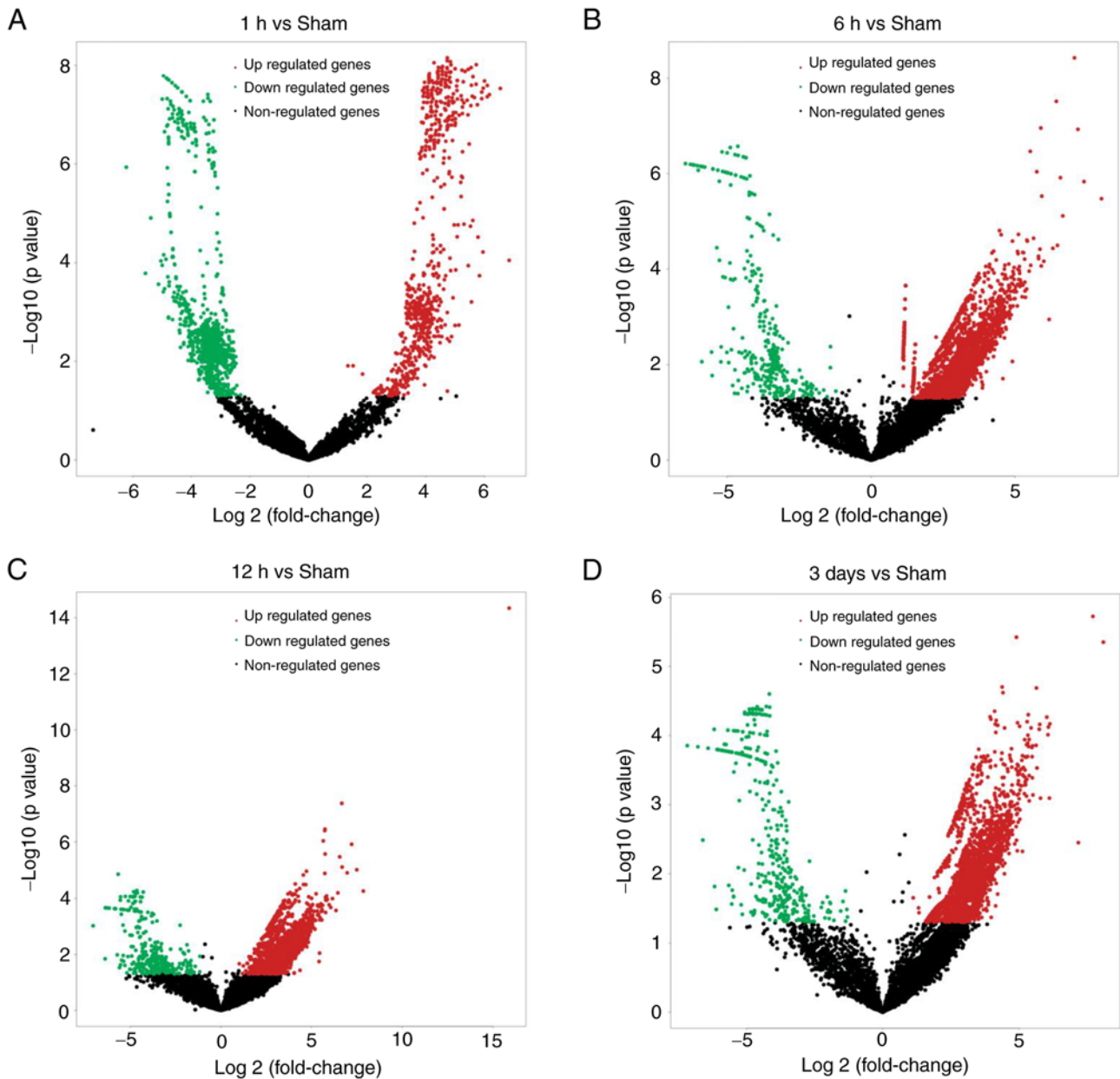


Figure 2. Expression profile of circRNAs during deep vein thrombosis development. (A-D) Volcano plot showed upregulated (red dot) and downregulated (green dot) circRNAs at the four time points. (A) 1 h vs. the sham group. (B) 6 h vs. the sham group. (C) 12 h vs. the sham group. (D) 3 days vs. the sham group. circRNAs, circular RNAs.

pathways in the enrichment analysis annotated by mRNA profile 45 were selected and searched for their input genes (Table II). The input genes in the platelet-associated pathway intersected with the annotated genes in profile 45, and four genes were obtained: α 4A-tubulin (Tuba4a), kinesin-8 (Kif18a), kinesin-4 (Kif4a) and galactose-binding protein (Lgals3 bp). According to the mRNA-circRNA interaction network of the four genes, 328 circRNAs interacting with the four mRNAs were obtained (Fig. 8A). The circRNAs in the early formation of DVT were first observed. The upregulated circRNAs at 1 and 6 h after model establishment, according to Venn analysis, and eight circRNAs were obtained (Fig. 8B). Two other circRNAs (CBT15_circR_40422 and CBT15_circR_22738) were found to interact with Kif18a, Kif4a, and Lgals3 bp. Therefore, these two circRNAs are also listed as candidate

circRNAs. On the basis of the aforementioned analysis, a total of ten circRNAs and four mRNAs were selected as candidates for further RT-qPCR verification (Table III).

Validation of the differential expression of candidate circRNAs and mRNAs by RT-qPCR. On the basis of the sequences of circRNAs, we designed primers for the candidate circRNAs across a splice site (back-splice), owing to the loop forming characteristic of the circRNAs. Primer 5.0 was used to design specific primers for candidate mRNAs and circRNAs (primer sequences are listed in Table I).

The expression of the ten circRNAs and four mRNAs was verified by RT-qPCR. The expression of nine of the ten circRNAs and all four mRNAs was consistent with the sequencing results, and CBT15_circR_2763 was discarded

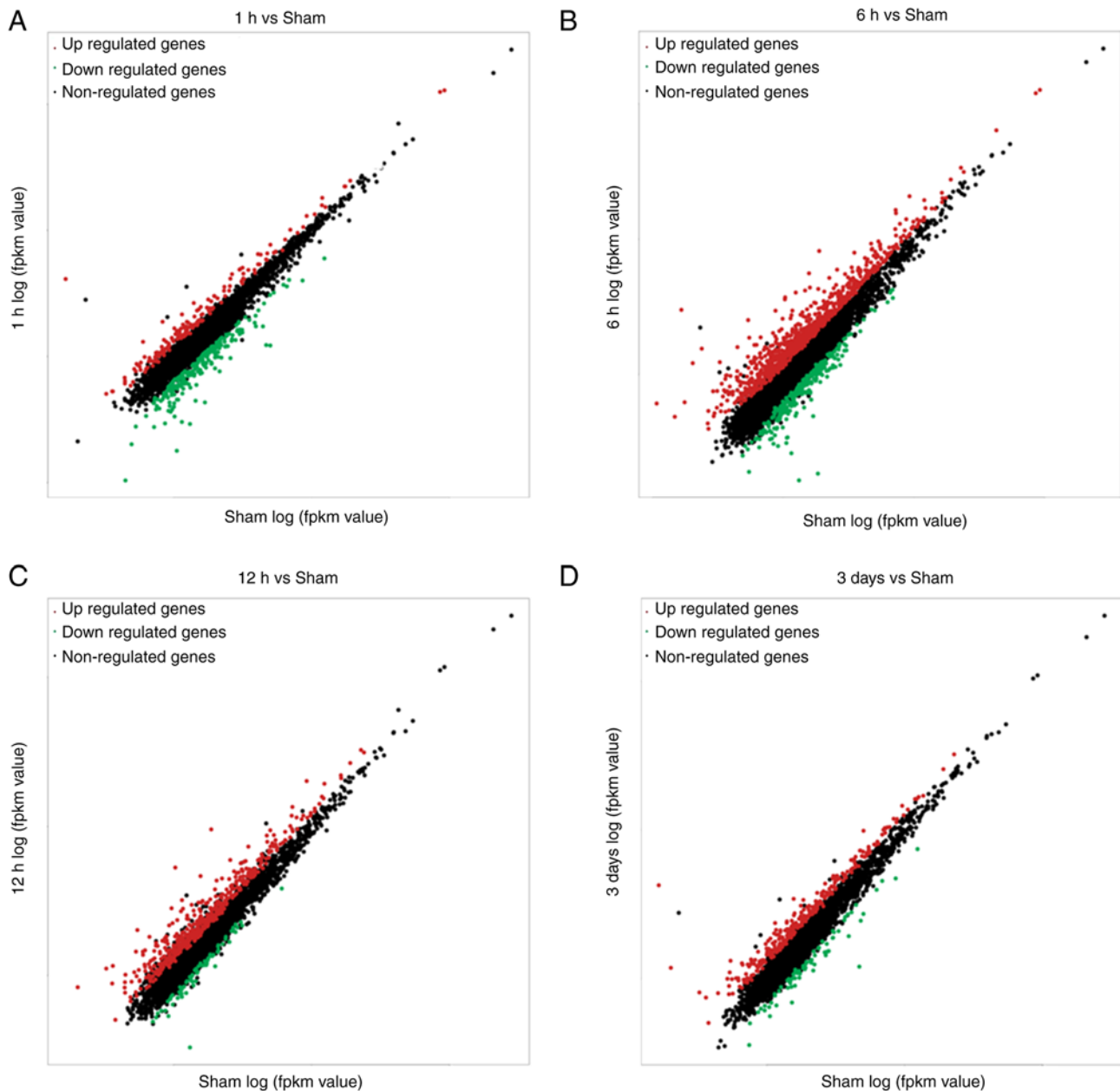


Figure 3. Expression profile of mRNAs during deep vein thrombosis development. (A-D) Scatterplots showed upregulated (red dot) and downregulated (green dot) circular RNAs at the four time points. (A) 1 h vs. the sham. (B) 6 h vs. the sham. (C) 12 h vs. the sham. (D) 3 days vs. the sham.

due to the large discrepancy between samples and the instability of the results (Fig. 9).

Discussion

Previous studies have suggested that surgical trauma and venous stasis are the main causative factors of DVT (25,26). Venous blood in the legs is prone to stasis in patients undergoing long-term bed rest or immobilization, thus resulting in hypoxia of the venous sinus, whereas blood stasis and hypoxia promote each other. Activation of venous endothelial cells and exogenous coagulation pathways ultimately leads to thrombosis. In the present study, a stenosis-induced rat model DVT was used to reflect the common clinical causes of DVT, such as postoperative immobilization, clinical trauma, or limb dysfunction. Brill *et al* (18) reported thrombus formation at

2 h in the stenosis model, and a thrombus-formation rate of 100% at 2 h in the DVT model rats of the present study was observed. Therefore, in order to observe further the DVT formation, two time points of 1 and 0.5 h were assessed. No clear clots at 1 h after surgery were observed but microthrombi in the partial ligated vessels after separation and washing were detected, as confirmed by H&E staining. The total thrombus-formation rate was 75% at 1 h. However, there was no evidence of any thrombosis at the 0.5-h time point. The difference in thrombus-initiation times between studies may have been associated with differences in manipulation and surgical instruments among laboratories, and differences in the immune status of the rats.

In the present study, the rate of thrombus formation in the model rats was 100% from 2 h to 3 days. On day 3, the thrombi became hard and began to organize, and clear organization was

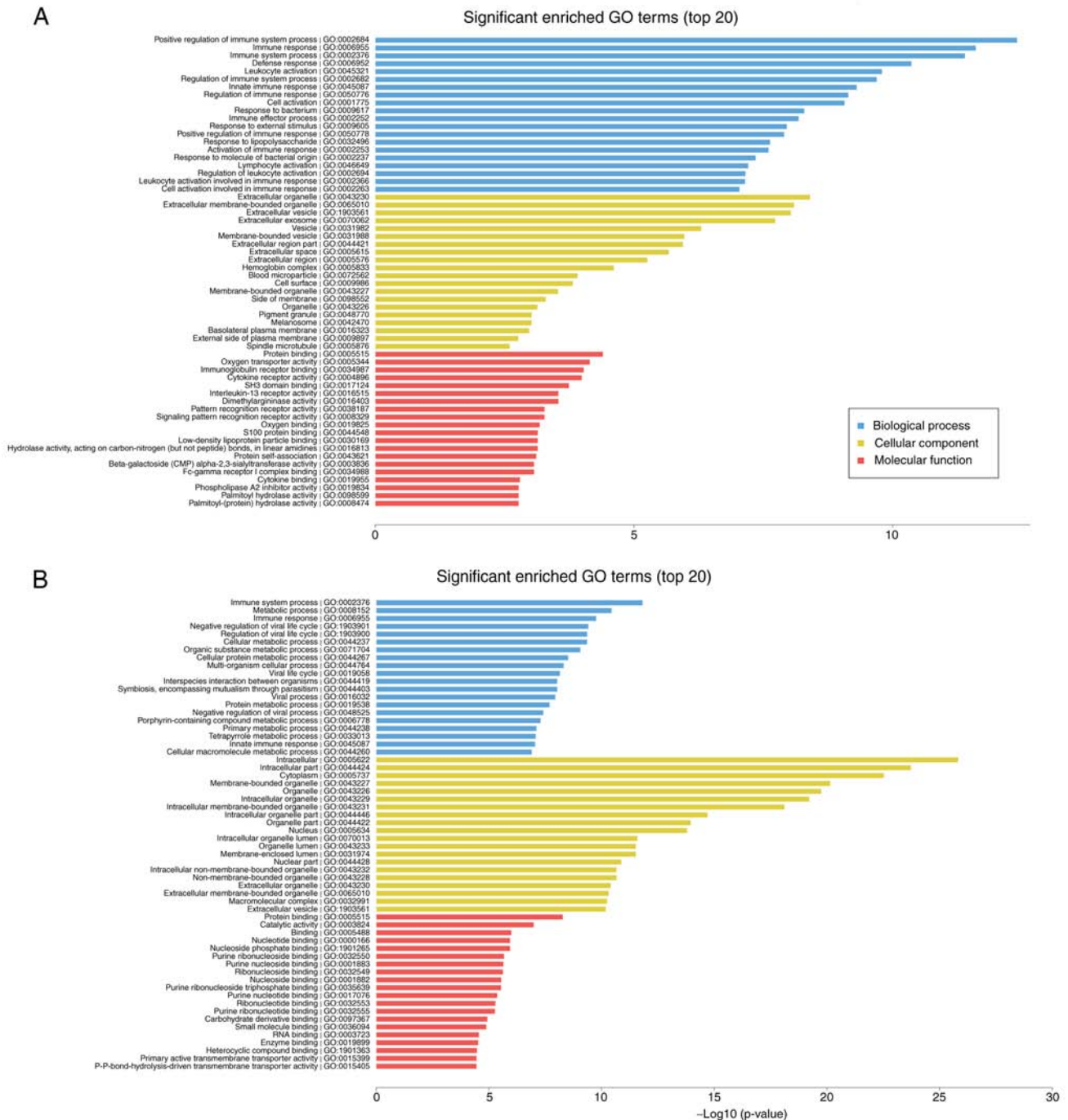


Figure 4. Continued.

observed by day 7. By day 21, some thrombi had disappeared, and the IVC had reopened. Thus, the present study revealed the entire process of thrombus development from initiation, through stability, to regression, and additionally analyzed thrombus weight and length. No thrombi were found in the sham group. These results indicated that the IVC thrombosis model was established successfully and displayed the entire process of thrombus evolution.

Moreover, it was revealed that microthrombi began to form in the ligated vessels at 1 h after operation. The thrombi formed rapidly in 1-6 h, were almost completely formed at 6 h, and reached a peak at 12 h after surgery. Subsequently, drying and recanalization of the thrombi were observed at 3 d after

operation. Hence, the DVT model rats were divided into four groups to explore in an improved way the roles of circRNAs and mRNAs in the different stages, and their related functions in the development of DVT.

To observe the dynamic changes in circRNAs and mRNAs in the development of the DVT rat model, RNA sequencing was performed to determine the circRNAs and mRNAs significantly differentially expressed in peripheral blood in the 1, 6 and 12 h, and 3-day groups compared with the sham group. GO and KEGG pathway analyses were then performed to predict their biological functions. The circRNA-mRNA regulatory network was established. Subsequently, RT-qPCR was conducted, and the results were consistent with the RNA sequencing results.

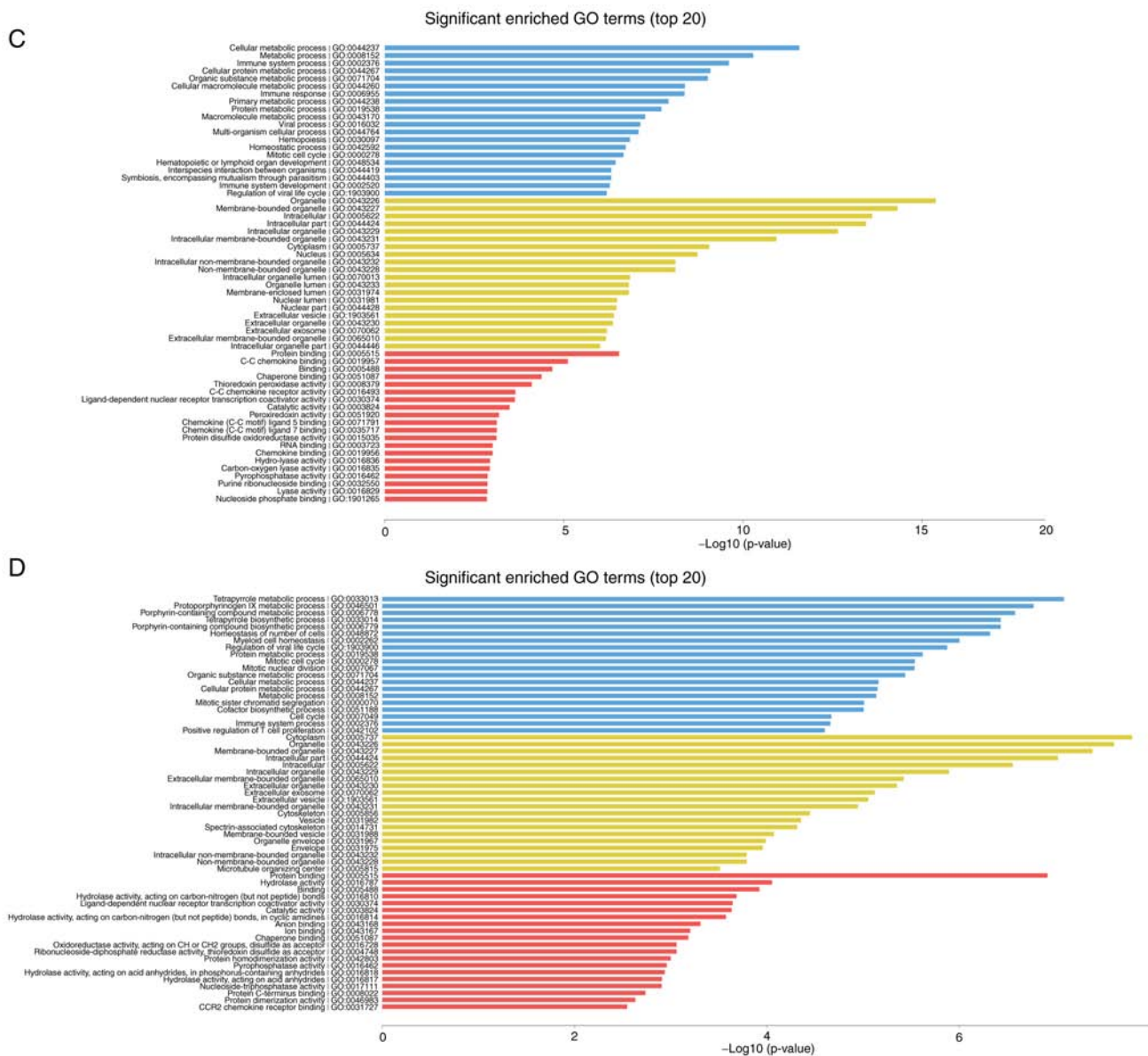


Figure 4. GO analysis of differentially expressed mRNAs at different stages of DVT rat models. The top 20 GO annotations of differentially expressed mRNAs between the group of DVT rat and the sham are shown. (A) 1 h vs. the sham. (B) 6 h vs. the sham. (C) 12 h vs. the sham. (D) 3 days vs. the sham. (A-D) GO analysis describing the possible functions of differentially expressed genes through the BP, CC and MF categories. Green indicates the BP, blue indicates the CC, and red indicates the MF. GO, Gene Ontology; DVT, deep vein thrombosis; BP, biological process; CC, cellular component; MF, molecular function.

Studies have shown that circRNAs are closely associated with cardiovascular diseases (27-30). In the present study, the entire progression of circRNAs in a DVT animal model, was effectively observed. According to the sequencing results, 1,680, 4,018, 3,724 and 3,036 circRNAs were differentially expressed in model rats at 1, 6 and 12 h, and 3 days, respectively, with respect to rats in the sham group. The number of upregulated circRNAs increased from 736 at 1 h to 3,691 at 6 h, then decreased slightly to 3,406 concurrently with thrombus stabilization at 12 h, and decreased further to 2,639 at 3 days, when the thrombi began to organize. During the entire process, the number of downregulated circRNAs was markedly lower than that of upregulated circRNAs at the three time points (6 h: 327; 12 h: 318; 3 days: 397). In view of this phenomenon, it was hypothesized that the upregulated circRNAs may have strongly responded to the stimulus of the

surgery used to establish the model. This result also demonstrated that circRNAs are involved in the occurrence and development of DVT.

Previous studies revealed that PAI-1 (SERPINE1 gene) and other fibrinolytic genes, such as PLG, PLAT, PLAU, SERPINF2, SERPINB2 and CPB2, are associated with VTE risk in humans (31,32). Anticoagulation and coagulation genes are natural candidate genes for VTE (33). Moreover, Mendelian randomization analysis indicated causal associations of vWF (34), SERPINE1, EPHB4, TYRO3, TNFRSF11A, BOC and CHI3L1 with VTE risk. In a recent study, authors have validated that thrombomodulin is involved in the evolution of DVT and can be used as a dynamic biomarker to measure disease activity (35). However, the present study globally investigated the dynamic expression of mRNA in the development of DVT. A total of 400, 1,176,

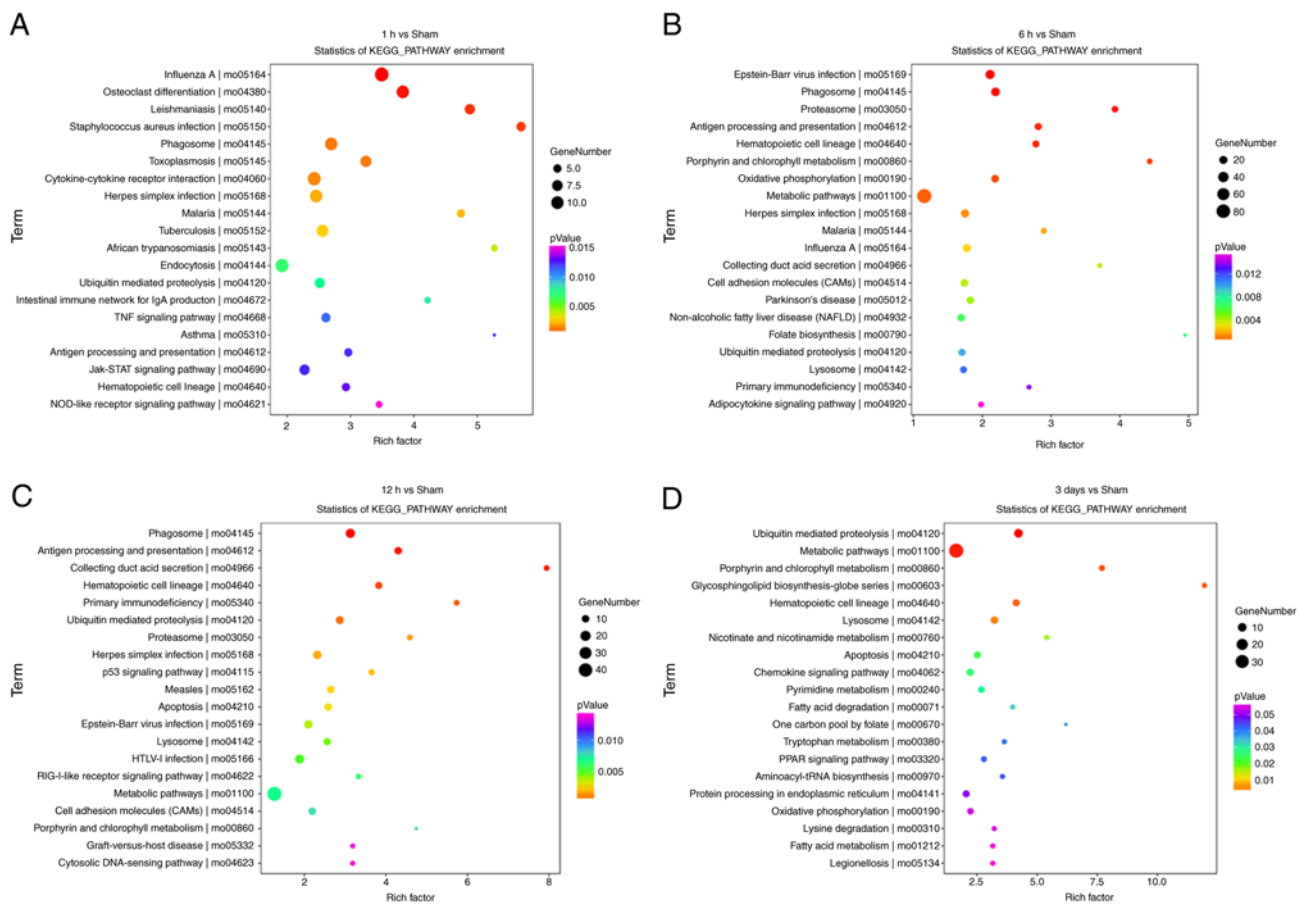


Figure 5. KEGG signaling pathways of differentially expressed mRNAs at different stages in DVT rat models. The top 20 KEGG pathways of differentially expressed mRNAs between the group of DVT rat and the sham are shown. (A) 1 h vs. the sham. (B) 6 h vs. the sham. (C) 12 h vs. the sham. (D) 3 days vs. the sham. (A-D) X-axis indicates the rich factor. The size of the bubble indicates the number of differentially expressed mRNAs enriched in the indicated pathway. DVT, deep vein thrombosis; KEGG, Kyoto Encyclopedia of Genes and Genomes.

373 and 573 differentially expressed mRNAs were identified in the 1, 6, and 12 h, and 3-day groups, respectively, vs. the sham group. The results indicated that 169, 885, 298 and 500 mRNAs were upregulated, and 231, 291, 75 and 73 mRNAs were downregulated. The sum of 69 upregulated mRNAs were identified at four time points, but no downregulated mRNAs were identified, according to Venn analysis. Certain targets were associated with DVT pathogenesis, such as vWF, ICAM-1, VCAM-1, ROS, HIF1 α , VEGFB, C-reactive protein, TF, CXCL12, MDM2 and MMP13. This discovery may provide a foundation for future mechanistic and clinical studies to advance understanding of the molecular etiology of DVT.

STEM analysis can cluster, compare and visualize gene expression data for short time series, and reveal their expression trends at different times, to help identify significantly expressed genes. From a biological perspective, genes with similar expression patterns may have common characteristics (36). STEM analysis to determine the temporal trends of the differentially expressed circRNAs and mRNAs was utilized. The STEM trends for mRNAs (profile 45) were consistent with those for circRNAs (also profile 45), consistently with the development of thrombosis in DVT rats, thereby confirming a positive interaction between circRNAs and mRNAs (37,38).

Enrichment analysis annotated by profile 45 identified several distinct pathways closely associated with thrombosis, including the platelet-associated pathway, inflammation-associated pathway, and immune-associated pathway. Platelets are a known component of venous thrombi (39). A previous study examining the role of platelets in venous thrombosis by using an *in vivo* model of venous valvular stasis has suggested that platelets adhere, activate, and subsequently promote thrombus growth beyond the valve sinus and toward the volumetric flow (40). In the present study, blood stasis was successfully induced, and multiple pathways associated with platelets were screened with enrichment assays, whose results were consistent with previous findings. To this day, increasing evidence supports the role of inflammation in thromboembolism (41). In patients with idiopathic DVT, inflammatory markers have been observed to persist (42). Increased membrane ICAM-1, P-selectin, and vWF, and impaired anticoagulant function have been reported to favor the recruitment of leukocytes and platelets, thus improving thrombus formation (43). vWF is expressed early in DVT and is key for platelet recruitment and the initiation of thrombosis in flow disturbance-driven thrombosis models (18). In the present study, inflammatory-associated pathways and differentially expressed inflammatory cytokines were also identified. The discovery of multiple pathways further

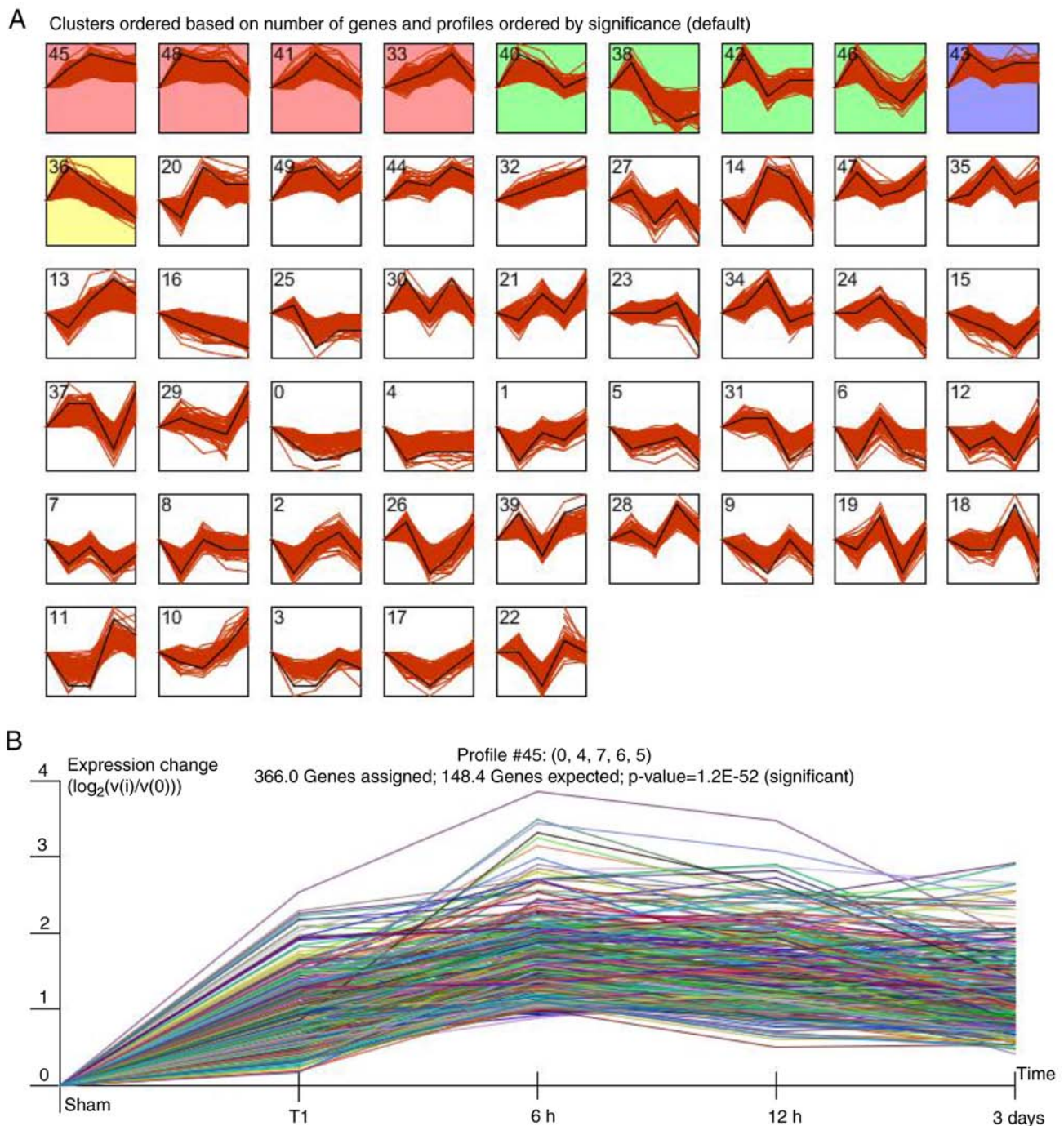


Figure 6. STEM analysis of differential expression of circular RNAs at different stages. (A) STEM analysis identified 10 significantly expressed profiles with $P < 0.05$. The black line in each profile represents the expression pattern of the genes at different times. (B) Expression patterns of profile 45. STEM, short time series expression miner.

demonstrated the results of multiple factors of thrombosis (44,45). However, the important roles and mechanisms of key circRNAs and mRNAs in these pathways in DVT progression, and whether the network relationship between these pathways promotes DVT development, have to be further studied in the future.

Because platelet activation is directly associated with thrombosis, four key genes were discovered during the first study of the platelet-associated pathway-Tuba4a, Kif18a, Kif4a and Lgals3bp-directly or indirectly associated with platelet production or activation, thrombosis, or cardiovascular

diseases. Notably, Tuba4a plays an important role in platelet biosynthesis and cardiovascular diseases (46-51).

To increase the likelihood of screening functional circRNAs, candidate circRNAs was identified according to mRNA-circRNA interaction relationships, on the basis of mRNA enrichment analysis, rather than simply relying on the expression fold change of the circRNAs. With RT-qPCR, nine out of ten circRNAs were verified; and it was further established that three of the circRNAs were annotated in CIRCpedia-V2, a rat circRNA database, thus confirming the presence of the three circRNAs. However, the lack of

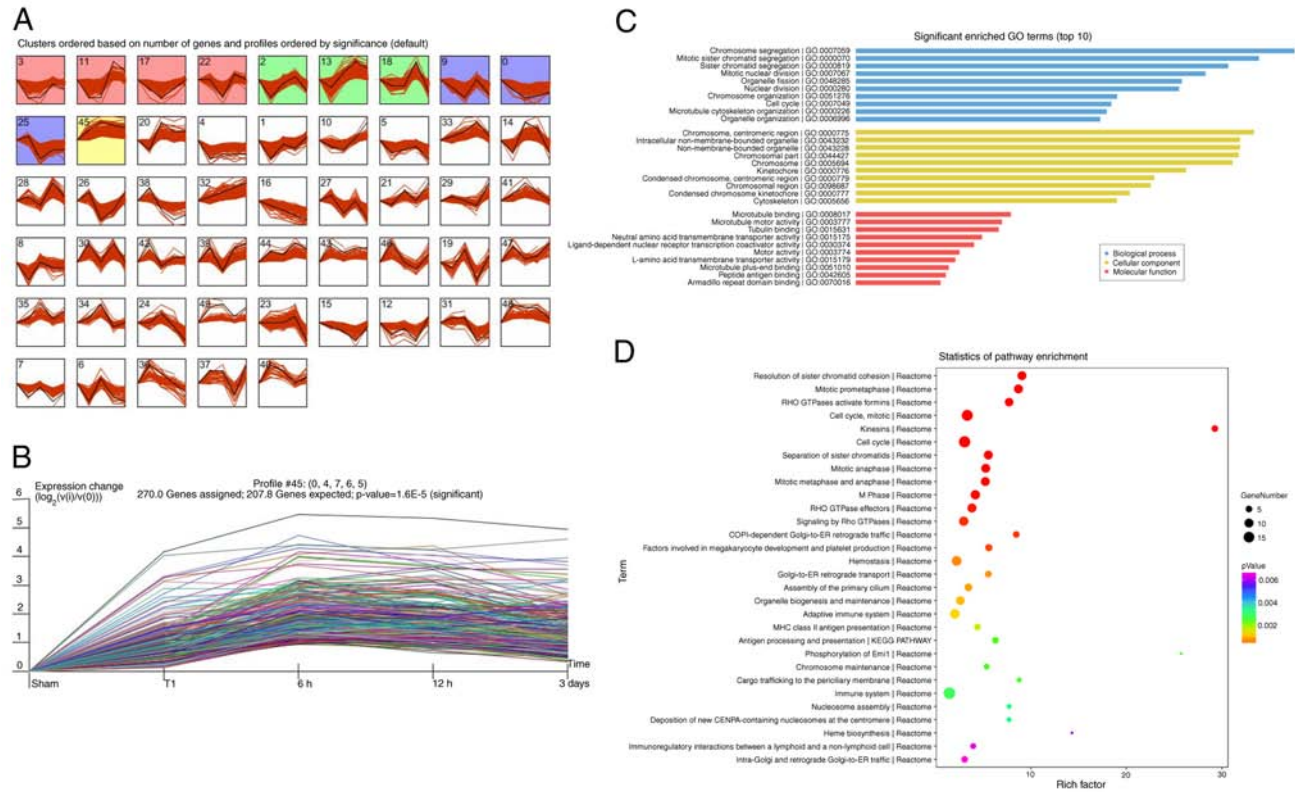


Figure 7. STEM analysis of differentially expression of mRNAs at different stages. (A) STEM analysis identified 11 significantly expressed profiles with $P < 0.05$. The black line in each profile represents the expression pattern of the genes at different times. (B) Expression patterns of Profile 45. (C) Gene Ontology analysis of Profile 45 using the BP, CC and MF categories. Green indicates the biological process, blue indicates the cellular component, and red indicates the MF. (D) Top 20 Kyoto Encyclopedia of Genes and Genomes pathways of Profile 45. X-axis indicates the risk factors. The size of the bubble indicates the number of genes enriched in the indicated pathway. STEM, short time series expression miner; BP, biological process; CC, cellular component; MF, molecular function.

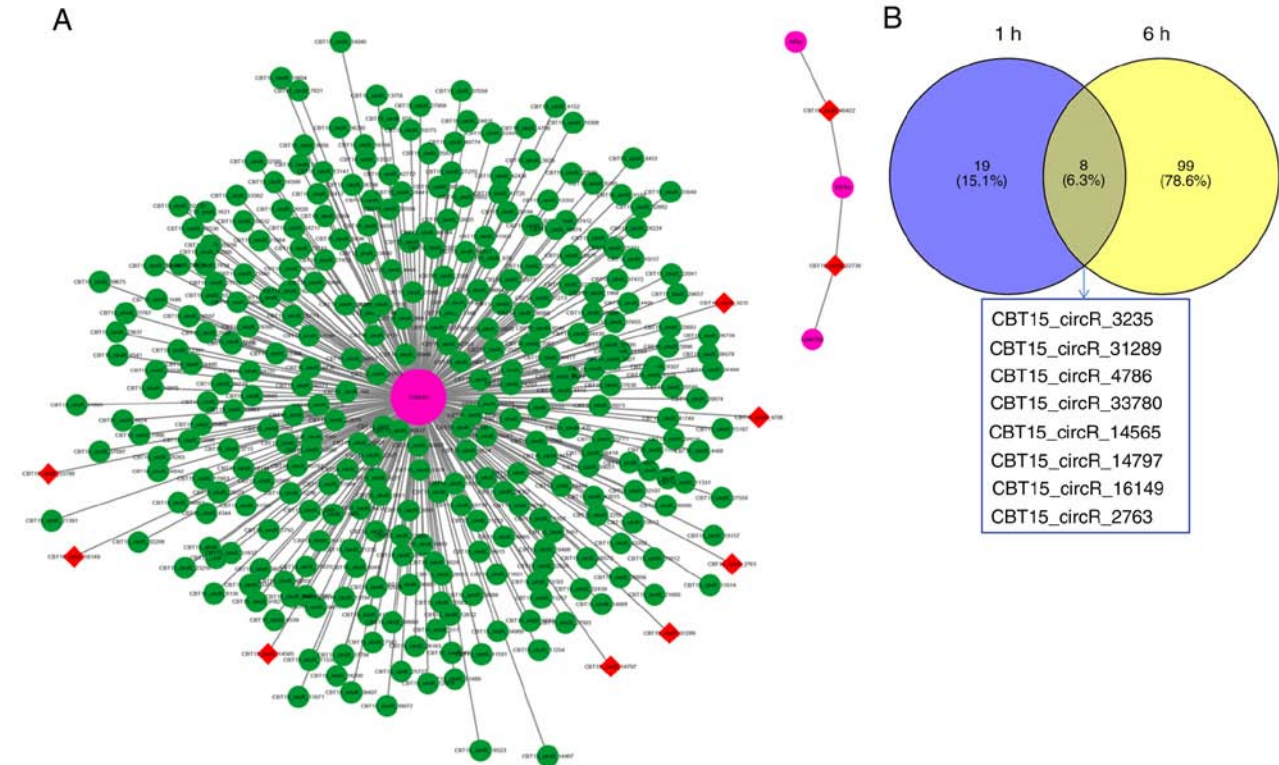


Figure 8. Screening of candidate circRNAs and mRNAs. (A) Construction of the circRNA-mRNA interaction network four mRNAs, including Tuba4a, Kif18a, Kif4a and Lgals3bp. Red circles indicate mRNAs, green circles indicate interacting circRNAs, red squares indicate the selected circRNAs. The grey lines indicated the relationship between circRNA and mRNA. (B) Venn analysis showed common upregulated circRNAs at 1 and 6 h. circRNA, circular RNA.

Table II. Platelet-related pathways and input gene.

Term	Input gene
Factors involved in megakaryocyte development and platelet production	Kif22, Kif18a, Racgap1, Kif4a, Kif2c
Platelet degranulation	Lgals3bp, Tuba4a
Response to elevated platelet cytosolic Ca ²⁺	Lgals3bp, Tuba4a
Platelet activation, signaling and aggregation	Lgals3bp, Tuba4a
Platelet activation	Itga2

Table III. Details of the 10 candidate circRNAs.

Running number	LogFC	P-value	Regulation	Chromosome	Length, bp
CBT15_circR_3235*	5.55	0.000624151	Up	Chr1: 255608044-255612190	4,146
CBT15_circR_31289	4.43	1.31112x10 ⁻⁸	Up	Chr5: 152377689-152378376	687
CBT15_circR_4786	4.35	2.11468x10 ⁻⁷	Up	Chr10: 106731880-106738104	6,224
CBT15_circR_33780	3.83	0.000489196	Up	Chr6: 21980222-21980905	683
CBT15_circR_14797	2.39	0.035099441	Up	Chr15: 52308036-52308580	544
CBT15_circR_2763	2.21	0.042581092	Up	Chr1: 235759863-235761819	1,956
CBT15_circR_14565	2.47	0.031028548	Up	Chr15: 41976569-41976792	223
CBT15_circR_16149	4.51	1.90551E-05	Up	Chr16: 73687145-73690537	3,392
CBT15_circR_40422	0.31	0.764794424	No	Chr8: 90482738-90483077	339
CBT15_circR_22738	-0.311230182	0.796548004	No	Chr2: 229005941-29006321	380

Circ, circular; FC, fold-change.

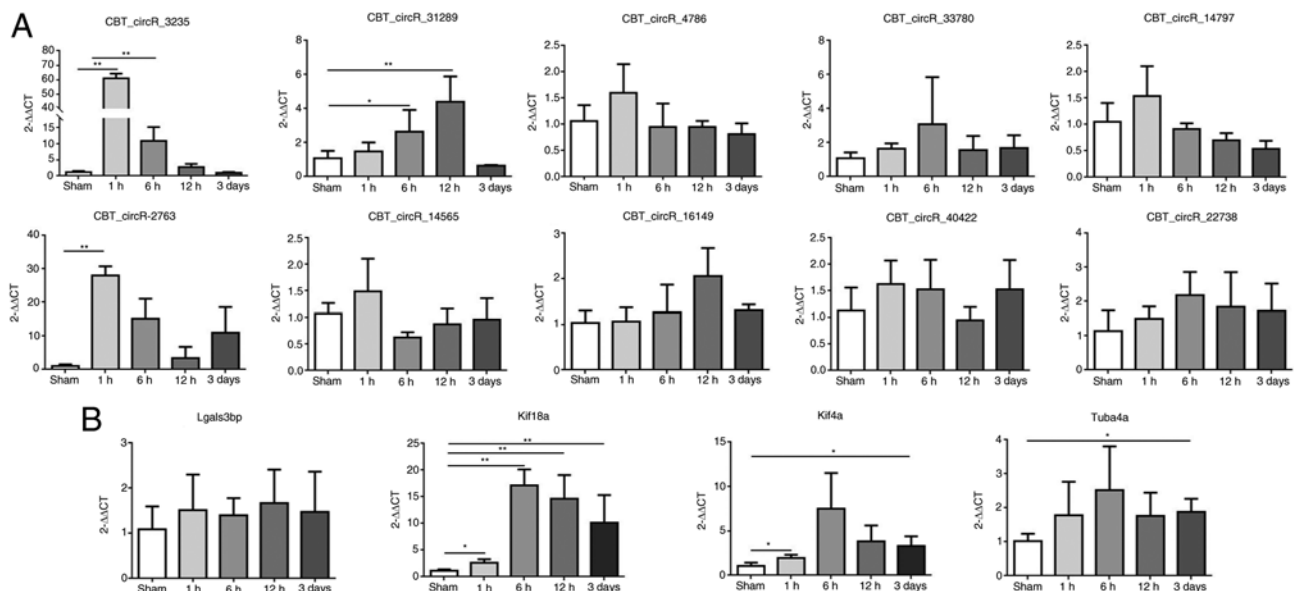


Figure 9. Validation of candidate circRNAs and mRNAs. (A) The expression level of candidate circRNAs by RT-qPCR. (B) The expression level of candidate mRNAs by RT-qPCR. *P<0.05 and **P<0.01. circRNA, circular RNA; RT-qPCR, quantitative reverse transcription PCR.

validation with western blotting and functional confirmation is a limitation of the present study.

Lou *et al* (16) have found that hsa_circ_000455 is a new circRNA biomarker for DVT in patients, according to microarray profiling. Their findings have indicated that certain circRNAs

can be used as indicators of DVT. At present, the expression of the circRNA in patients with DVT was also observed, by identifying its human homolog according to the circBase database. The expression of the human homologous circRNA in the peripheral blood of 21 patients with DVT was detected by RT-qPCR. The

results revealed significantly higher human homologous circRNA expression levels in the DVT group than the control group. Receiver Operating Characteristic analysis of 21 patients with identified circRNA expression revealed an area under the curve of 0.897 with a sensitivity of 83.3% and a specificity of 95.4% (data not shown). These results showed preliminarily favorable diagnostic performance. In addition, because the identified circRNAs in the present study are the circRNAs at 1 and 6 h after model establishment, which are at early stage in the evolution of thrombosis, it is considered that the circRNAs could be used as indicators of DVT at the early stage, although the results need to be further verified by expanding the sample.

In summary, in the present study a rat model of DVT through the stenosis method was successfully established. This model demonstrated the entire evolution of DVT. Through RNA sequencing, the circRNA and mRNA expression profile trends were thoroughly observed. This preliminarily study explored the global expression profiles of circRNAs and mRNAs in the progression of DVT. Competing endogenous RNA (ceRNA) is not a specific type of RNA but a regulatory mechanism, wherein miRNA binds target mRNA and consequently engages in post-transcriptional gene regulation by inhibiting the mRNA's translation or degradation. CircRNA binds miRNA through microRNA response elements, thus relieving the inhibitory effect of miRNA on mRNA and indirectly regulating mRNA expression. Therefore, circRNAs positively indirectly regulate gene expression and function through ceRNA mechanisms (52-54).

Future studies on the ceRNA relationships between circRNAs and mRNAs *in vitro* and *in vivo* are needed. The potential network regulation mechanism of circRNA-miRNA-mRNA was confirmed in the identified circRNA and mRNA analysis in DVT. According to the MiRdb and Targetscan databases, miRNAs binding both the circRNA and the mRNA were screened. In future studies, RNA fluorescence *in situ* hybridization assays will be performed to identify the subcellular localization of the circRNA and miRNA in human umbilical vein endothelial cells and dual-luciferase assays to verify the target relationship between the circRNA and the miRNA, and the miRNA and the mRNA. In addition, further studies are also necessary to discover the functions of the key circRNAs and their regulatory mechanisms in DVT development.

Acknowledgements

Not applicable.

Funding

The present study was supported by the Health Department Project of Jiangsu (grant no. Z2019003), the Nature Science Foundation of Nantong, Jiangsu (grant no. MS12021003), the Graduate Research and Practice Innovation Program of Jiangsu (grant no. KYCX20_2799) and the Jiangsu Provincial Medical Key Discipline (grant no. ZDXK202240).

Availability of data and materials

Transcriptome sequencing datasets generated and/or analyzed during the current study are available in the NCBI database

with accession code GSE148333 (<https://www.ncbi.nlm.nih.gov/geo/query/acc.cgi?acc=GSE148333>). The datasets used and/or analyzed during the current study are available from the corresponding author on reasonable request.

Authors' contributions

BS, XC and YQZ designed the experiments. BS, XC, MZ, QS and XXZ performed the experiments. BS, XC, XW and YQZ take responsibility for analysis accuracy of the whole experimental study. XW revised the manuscript. BS wrote the first draft of the manuscript and all authors commented on previous versions of the manuscript. BS and XC confirm the authenticity of all the raw data. All authors read and approved the final version of the manuscript.

Ethics approval and consent to participate

Animal experiments were conducted following the Chinese law on the protection of animals used for scientific purposes. Furthermore, the study was specifically approved (approval no. 20170930-001) by the Ethical Committee of Animal Experiments of Nantong University (Nantong, China). The study was carried out in compliance with the ARRIVE guidelines.

Patient consent for publication

Not applicable.

Competing interests

The authors declare that they have no competing interests.

References

1. Chopard R, Albertsen IE and Piazza G: Diagnosis and treatment of lower extremity venous thromboembolism: A review. *JAMA* 324: 1765-1776, 2020.
2. Heit JA, Spencer FA and White RH: The epidemiology of venous thromboembolism. *J Thromb Thrombolysis* 41: 3-14, 2016.
3. Wendelboe AM and Raskob GE: Global burden of thrombosis: Epidemiologic aspects. *Circ Res* 118: 1340-1347, 2016.
4. Maatman TK, Jalali F, Feizpour C, Douglas A II, McGuire SP, Kinnaman G, Hartwell JL, Maatman BT, Kreutz RP, Kapoor R, *et al*: Routine venous thromboembolism prophylaxis may be inadequate in the hypercoagulable state of severe coronavirus disease 2019. *Crit Care Med* 48: e783-e790, 2020.
5. Alexander M and Burbury K: A systematic review of biomarkers for the prediction of thromboembolism in lung cancer-results, practical issues and proposed strategies for future risk prediction models. *Thromb Res* 148: 63-69, 2016.
6. Memczak S, Jens M, Elefsinioti A, Torti F, Krueger J, Rybak A, Maier L, Mackowiak SD, Gregersen LH, Munschauer M, *et al*: Circular RNAs are a large class of animal RNAs with regulatory potency. *Nature* 495: 333-338, 2013.
7. Zhang Y, Zhang XO, Chen T, Xiang JF, Yin QF, Xing YH, Zhu S, Yang L and Chen LL: Circular intronic long noncoding RNAs. *Mol Cell* 51: 792-806, 2013.
8. Ashwal-Fluss R, Meyer M, Pamudurti NR, Ivanov A, Bartok O, Hanan M, Evantal N, Memczak S, Rajewsky N and Kadener S: circRNA biogenesis competes with pre-mRNA splicing. *Mol Cell* 56: 55-66, 2014.
9. Liu Y, Yang Y, Wang Z, Fu X, Chu XM, Li Y, Wang Q, He X, Li M, Wang K, *et al*: Insights into the regulatory role of circRNA in angiogenesis and clinical implications. *Atherosclerosis* 298: 14-26, 2020.
10. Chen S, Yang X, Yu C, Zhou W, Xia Q, Liu Y, Chen Q, Chen X, Lv Y and Lin Y: The potential of circRNA as a novel diagnostic biomarker in cervical cancer. *J Oncol* 2021: 5529486, 2021.

11. Aufiero S, Reckman YJ, Pinto YM and Creemers EE: Circular RNAs open a new chapter in cardiovascular biology. *Nat Rev Cardiol* 16: 503-514, 2019.
12. Wang K, Long B, Liu F, Wang JX, Liu CY, Zhao B, Zhou LY, Sun T, Wang M, Yu T, *et al*: A circular RNA protects the heart from pathological hypertrophy and heart failure by targeting miR-223. *Eur Heart J* 37: 2602-2611, 2016.
13. Ma C, Gu R, Wang X, He S, Bai J, Zhang L, Zhang J, Li Q, Qu L, Xin W, *et al*: circRNA CDR1as promotes pulmonary artery smooth muscle cell calcification by upregulating CAMK2D and CNN3 via sponging miR-7-5p. *Mol Ther Nucl Acids* 22: 530-541, 2020.
14. Zhao Z, Li X, Gao C, Jian D, Hao P, Rao L and Li M: Peripheral blood circular RNA hsa_circ_0124644 can be used as a diagnostic biomarker of coronary artery disease. *Sci Rep* 7: 39918, 2017.
15. Yi YY, Yi Y, Zhu X, Zhang J, Zhou J, Tang X, Lin J, Wang P and Deng ZQ: Circular RNA of vimentin expression as a valuable predictor for acute myeloid leukemia development and prognosis. *J Cell Physiol* 234: 3711-3719, 2019.
16. Lou Z, Li X, Li C, Li X, Du K, Zhang F and Wang B: Microarray profile of circular RNAs identifies hsa_circ_000455 as a new circular RNA biomarker for deep vein thrombosis. *Vascular* 30: 577-589, 2022.
17. Lou Z, Ma H, Li X, Zhang F, Du K and Wang B: Hsa_circ_0001020 accelerates the lower extremity deep vein thrombosis via sponging miR-29c-3p to promote MDM2 expression. *Thromb Res* 211: 38-48, 2022.
18. Brill A, Fuchs TA, Chauhan AK, Yang JJ, De Meyer SF, Köllnberger M, Wakefield TW, Lämmle B, Massberg S and Wagner DD: von Willebrand factor-mediated platelet adhesion is critical for deep vein thrombosis in mouse models. *Blood* 117: 1400-1407, 2011.
19. Diaz JA, Hawley AE, Alvarado CM, Berguer AM, Baker NK, Wroblewski SK, Wakefield TW, Lucchesia BR and Myers DD Jr: Thrombogenesis with continuous blood flow in the inferior vena cava. A novel mouse model. *Thromb Haemostasis* 104: 366-375, 2010.
20. Langmead B, Trapnell C, Pop M and Salzberg SL: Ultrafast and memory-efficient alignment of short DNA sequences to the human genome. *Genome Biol* 10: R25, 2009.
21. Ritchie ME, Phipson B, Wu D, Hu Y, Law CW, Shi W and Smyth GK: limma powers differential expression analyses for RNA-sequencing and microarray studies. *Nucleic Acids Res* 43: e47, 2015.
22. Wu T, Hu E, Xu S, Chen M, Guo P, Dai Z, Feng T, Zhou L, Tang W, Zhan L, *et al*: clusterProfiler 4.0: A universal enrichment tool for interpreting omics data. *Innovation (Camb)* 2: 100141, 2021.
23. Livak KJ and Schmittgen TD: Analysis of relative gene expression data using real-time quantitative PCR and the 2(-Delta Delta C(T)) method. *Methods* 25: 402-408, 2001.
24. Panova-Noeva M, Wagner B, Nagler M, Koeck T, Ten Cate V, Prochaska JH, Heitmeier S, Meyer I, Gerdes C, Laux V, *et al*: Comprehensive platelet phenotyping supports the role of platelets in the pathogenesis of acute venous thromboembolism-results from clinical observation studies. *EBioMedicine* 60: 102978, 2020.
25. Bovill EG and van der Vliet A: Venous valvular stasis-associated hypoxia and thrombosis: What is the link? *Annu Rev Physiol* 73: 527-545, 2011.
26. Mackman N: New insights into the mechanisms of venous thrombosis. *J Clin Invest* 122: 2331-2336, 2012.
27. Vilades D, Martínez-Camblor P, Ferrero-Gregori A, Bär C, Lu D, Xiao K, Vea A, Nasarre L, Sanchez Vega J, Leta R, *et al*: Plasma circular RNA hsa_circ_0001445 and coronary artery disease: Performance as a biomarker. *FASEB J* 34: 4403-4414, 2020.
28. Ryu J, Kwon DH, Choe N, Shin S, Jeong G, Lim YH, Kim J, Park WJ, Kook H and Kim YK: Characterization of circular RNAs in vascular smooth muscle cells with vascular calcification. *Mol Ther Nucl Acids* 19: 31-41, 2020.
29. Su Q and Lv X: Revealing new landscape of cardiovascular disease through circular RNA-miRNA-mRNA axis. *Genomics* 112: 1680-1685, 2020.
30. Ge X, Meng Q, Zhuang R, Yuan D, Liu J, Lin F, Fan H and Zhou X: Circular RNA expression alterations in extracellular vesicles isolated from murine heart post ischemia/reperfusion injury. *Int J Cardiol* 296: 136-140, 2019.
31. Lindström S, Wang L, Smith EN, Gordon W, van Hylckama Vlieg A, de Andrade M, Brody JA, Pattee JW, Haessler J, Brumpton BM, *et al*: Genomic and transcriptomic association studies identify 16 novel susceptibility loci for venous thromboembolism. *Blood* 134: 1645-1657, 2019.
32. Klarin D, Busenkell E, Judy R, Lynch J, Levin M, Haessler J, Aragam K, Chaffin M, Haas M, Lindström S, *et al*: Genome-wide association analysis of venous thromboembolism identifies new risk loci and genetic overlap with arterial vascular disease. *Nat Genet* 51: 1574-1579, 2019.
33. Zöller B, Svensson PJ, Dahlbäck B, Lind-Hallden C, Hallden C and Elf J: Genetic risk factors for venous thromboembolism. *Expert Rev Hematol* 13: 971-981, 2020.
34. Yuan S, Titova OE, Zhang K, Gou W, Schillemans T, Natarajan P, Chen J, Li X, Åkesson A, Bruzelius M, *et al*: Plasma protein and venous thromboembolism: Prospective cohort and mendelian randomisation analyses. *Br J Haematol* 201: 783-792, 2023.
35. Cheng X, Sun B, Liu S, Li D, Yang X and Zhang Y: Identification of thrombomodulin as a dynamic monitoring biomarker for deep venous thrombosis evolution. *Exp Ther Med* 21: 142, 2021.
36. Ernst J and Bar-Joseph Z: STEM: A tool for the analysis of short time series gene expression data. *BMC Bioinformatics* 7: 191, 2006.
37. Navarro E, Mallén A, Cruzado JM, Torras J and Hueso M: Unveiling ncRNA regulatory axes in atherosclerosis progression. *Clin Transl Med* 9: 5, 2020.
38. Li M, Duan L, Li Y and Liu B: Long noncoding RNA/circular noncoding RNA-miRNA-mRNA axes in cardiovascular diseases. *Life Sci* 233: 116440, 2019.
39. Stone J, Hangge P, Albadawi H, Wallace A, Shamoun F, Knuttien MG, Naidu S and Oklu R: Deep vein thrombosis: Pathogenesis, diagnosis, and medical management. *Cardiovasc Diagn Ther* 7 (Suppl 3): S276-S284, 2017.
40. Lehmann M, Schoeman RM, Krohl PJ, Wallbank AM, Samaniuk JR, Jandrot-Perrus M and Neeves KB: Platelets drive thrombus propagation in a hematocrit and glycoprotein VI-dependent manner in an in vitro venous thrombosis model. *Arterioscler Thromb Vasc Biol* 38: 1052-1062, 2018.
41. Saghaizadeh A, Hafizi S and Rezaei N: Inflammation in venous thromboembolism: Cause or consequence? *Int Immunopharmacol* 28: 655-665, 2015.
42. Poredos P and Jezovnik MK: In patients with idiopathic venous thrombosis, interleukin-10 is decreased and related to endothelial dysfunction. *Heart Vessels* 26: 596-602, 2011.
43. Budnik I and Brill A: Immune factors in deep vein thrombosis initiation. *Trends Immunol* 39: 610-623, 2018.
44. Parakh RS and Sabath DE: Venous thromboembolism: Role of the clinical laboratory in diagnosis and management. *J Appl Lab Med* 3: 870-882, 2019.
45. Najem MY, Couturaud F and Lemarié CA: Cytokine and chemokine regulation of venous thromboembolism. *J Thromb Haemostasis* 18: 1009-1019, 2020.
46. Strassel C, Magiera MM, Dupuis A, Batzenschlager M, Hovasse A, Pleines I, Guéguen P, Eckly A, Moog S, Mallo L, *et al*: An essential role for α 4-tubulin in platelet biogenesis. *Life Sci Alliance* 2: e201900309, 2019.
47. Feng L, Yang X, Asweto CO, Wu J, Zhang Y, Hu H, Shi Y, Duan J and Sun Z: Genome-wide transcriptional analysis of cardiovascular-related genes and pathways induced by PM_{2.5} in human myocardial cells. *Environ Sci Pollut Res Int* 24: 11683-11693, 2017.
48. DeRoo EP, Wroblewski SK, Shea EM, Al-Khalil RK, Hawley AE, Henke PK, Myers DD Jr, Wakefield TW and Diaz JA: The role of galectin-3 and galectin-3-binding protein in venous thrombosis. *Blood* 125: 1813-1821, 2015.
49. Tang F, Pan MH, Wan X, Lu Y, Zhang Y and Sun SC: Kif18a regulates Sirt2-mediated tubulin acetylation for spindle organization during mouse oocyte meiosis. *Cell Div* 13: 9, 2018.
50. Kim S, Cho YB, Song CU, Eyun S and Seo YJ: Kinesin family member KIF18A is a critical cellular factor that regulates the differentiation and activation of dendritic cells. *Genes Genomics* 42: 41-46, 2020.
51. Nunes Bastos R, Gandhi SR, Baron RD, Gruneberg U, Nigg EA and Barr FA: Aurora B suppresses microtubule dynamics and limits central spindle size by locally activating KIF4A. *J Cell Bio* 202: 605-621, 2013.
52. Hansen TB, Jensen TI, Clausen BH, Bramsen JB, Finsen B, Damgaard CK and Kjems J: Natural RNA circles function as efficient microRNA sponges. *Nature* 495: 384-388, 2013.
53. Jeck WR, Sorrentino JA, Wang K, Slevin MK, Burd CE, Liu J, Marzluff WF and Sharpless NE: Circular RNAs are abundant, conserved, and associated with ALU repeats. *RNA* 19: 141-157, 2013.
54. Wilusz JE and Sharp PA: Molecular biology. A circuitous route to noncoding RNA. *Science* 340: 440-441, 2013.

